CAS Key Laboratory of Quantum Information, University of Science and Technology of China

Xiao-Yan Yang , Hai-Feng Zhang , Peng Duan * , Lei Du , Hao-Ran Tao , Liang-Liang Guo , Tian-Le Wang , Zhi-Long Jia , Wei-Cheng Kong , Guo-Ping Guo

Posted Date: 23 April 2024

doi: 10.20944/preprints202403.1706.v2

Keywords: quantum computation; microwave crosstalk; superconducting circuit

Article

Fast, Universal Scheme for Calibrating Microwave Crosstalk in Superconducting Circuits

Xiao-Yan Yang [1,2], Hai-Feng Zhang [1,2], Peng Duan [1,2,*], Lei Du [1,2], Hao-Ran Tao [1,2], Liang-Liang Guo [1,2], Tian-Le Wang [1,2], Zhi-Long Jia [3], Wei-Cheng Kong [3] and Guo-Ping Guo [1,2,3,*]

[1] AS Key Laboratory of Quantum Information, University of Science and Technology of China, Hefei, Anhui 230026, China
[2] CAS Center for Excellence and Synergetic Innovation Center in Quantum Information and Quantum Physics, University of Science and Technology of China, Hefei, Anhui 230026, China
[3] Origin Quantum Computing Company Limited, Hefei, Anhui 230026, China
* Correspondence: pengduan@ustc.edu.cn; gpguo@ustc.edu.cn

Abstract: A challenge in building large-scale superconducting quantum processors is the precise control and manipulation of the qubit state. However, the crosstalk between the microwave control lines impedes the parallel execution of high-fidelity digital and analog quantum operations. Here, we propose and demonstrate a universal compensation protocol for calibrating the microwave signal crosstalk. We also introduce amplified error sequences to optimize the accuracy. Furthermore, we show a definitive improvement in parallel gate operations with crosstalk cancellation, demonstrating the technique's effectiveness. This work paves the way for superconducting hardware that features automated calibration of microwave crosstalk, leading to enhanced fidelities in multiqubit circuits.

Keywords: quantum computation; microwave crosstalk; superconducting circuit

---

Quantum computing is promising for solving complex problems beyond the reach of traditional computing methods [1–3]. Despite recent demonstrations of quantum supremacy [4–10], utility [11], and quantum logical error correction [12–18], achieving scalable quantum computing is still obstructed by numerous challenges [19]. Among these, crosstalk is well-recognized in various quantum computing systems [20–28]. Specifically, microwave crosstalk in superconducting circuits significantly impacts system performance by inducing unwanted quantum state transitions and gate errors [29–32]. Figure1(a) shows such an example for transmon qubit, where the first three levels are included [33]. A microwave drive signal intended for bias qubit Q_b with Rabi strength Ω_b and frequency ω_{cr} couples unintentionally to target qubit, inducing an effective Rabi strength Ω_{cr} on the target qubit. $re^{i\phi_{cr}} = \Omega_{cr}/\Omega_b$ is the complex transfer amplitude or the so-called crosstalk coefficient. Leakage occurs when the frequency ω_{cr} of the spurious microwave signal is near resonance with the transition frequency ω_{ef} between the first excited ($|e\rangle$) and second excited ($|f\rangle$) states. Gate errors manifest when ω_{cr} is near resonance with the transition frequency ω_{ge} between the ground ($|g\rangle$) and the first excited ($|f\rangle$) state. This form of interference disrupts the precise control over qubit states which is essential for accurate quantum computation and error correction. As such, the characterization and mitigation of microwave crosstalk within superconducting circuits are critical for robust and scalable quantum computing architectures.

As microwave crosstalk can always be compensated with an additional out-of-phase signal, as shown in Figure1(a), the task translates to how one can characterize and calibrate the complex amplitude $re^{i\phi_{cr}}$ of the crosstalk signal, so a compensation signal of the same frequency and amplitude but out-of-phase can be applied to null the crosstalk signal. Some previous works have addressed this issue, each in a particular condition. When $\omega_{cr} = \omega_{ge}$, a clear constructive and destructive dynamic Rabi oscillation pattern is observed when ϕ_{cr} changes periodically [34,35], which can be used to extract r and ϕ_{cr}. Refs. [36,37] extended this method to off-resonant case ($\omega_{cr} \neq \omega_{ge}$) and Ref. [36] further provided an analytical formula to fit the oscillation pattern. For far-off resonance, the interference pattern of Rabi oscillation becomes invisible, and the spin-echo sequence is proposed [38] to calibrate microwave crosstalk utilizing the AC-Stark effect. Ref. [15] used the Ramsey error filter sequence to suppress leakage when ω_{cr} is in the vicinity of ω_{ef}. Although these schemes can cover a

 doi:10.20944/preprints202403.1706.v2

majority of crosstalk scenarios in the three-level subspace of transmon qubit, they are not universal and lack a unified model that governs the basic principle of the calibration procedure. Most of these schemes require at least one two-dimensional scan to obtain the final results, which makes it rather time-consuming to bring up a large quantum processor. Moreover, the sensitivity of these schemes is challenged when $|\omega_{cr} - \omega_{ge}| \gg 0$ or $|\eta|$, where $\eta = \omega_{ef} - \omega_{ge}$ is the anharmonicity of the superconducting qubit.

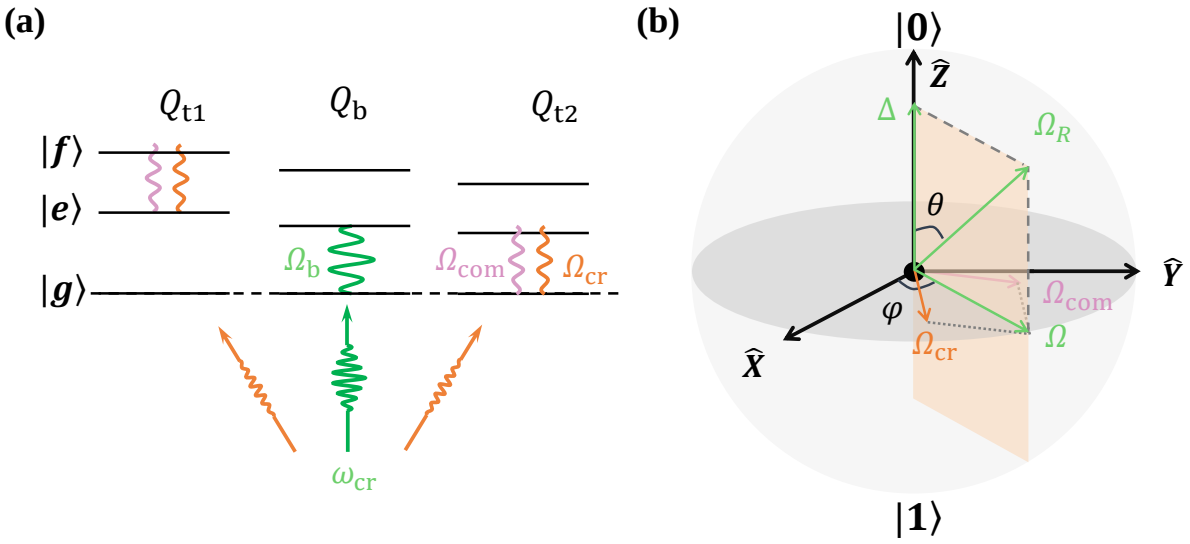

Figure 1. Schematic diagram of microwave crosstalk. (a) A microwave signal of frequency ω_{cr} intended to drive bias qubit Q_b with Rabi strength Ω_b, coupled unintentionally to some target qubits where a Rabi strength Ω_{cr} is induced. To nullify this crosstalk signal Ω_{cr}, an out-of-phase signal Ω_{com} should be applied directly on target qubits. (b) Bloch sphere representation of off-resonant driving Hamiltonian. The control fields of $\mathbf{\Omega}_{cr}$, $\mathbf{\Omega}_{com}$, and $\mathbf{\Delta}$ give effective control field $\mathbf{\Omega}_\mathbf{R}$ with angles θ from the $\mathbf{Z}$ axis and φ from the $\mathbf{X}$ axis.

Here, we propose and demonstrate a fast and universal scheme using Ramsey-like sequences for calibrating microwave crosstalk. Given the abovementioned limitations, this work contributes to the literature mainly from three aspects. First, we propose and experimentally validate a simple two-level off-resonant driving model; this theoretical model unifies the calibrating principle for all crosstalk scenarios and provides explicit formulas to fit the experimental data. Second, instead of requiring a two-dimensional parameter scanning procedure, only multiple one-dimensional sweeps are sufficient for accurately retrieving target parameters. Third, we introduce error-amplifying sequences to improve accuracy, especially in large detuning regions. With these advancements in terms of universality, efficiency, and accuracy, our method can be readily applied to a fully automated calibration of microwave crosstalk in a large-scale quantum processor. This approach helps to utilize the full potential of contemporary noisy-intermediate-scale quantum processors.

While superconducting qubits have multiple energy levels, a two-level-system (TLS) model is adequately comprehensive for addressing the issue of microwave crosstalk. In the presence of leakage, our focus is primarily on the $\{|e\rangle, |f\rangle\}$ subspace. Conversely, when gate errors occur, attention is directed toward the computational subspace, $\{|g\rangle, |e\rangle\}$. This simplification allows for a focused analysis of the phenomena critical to understanding and calibrating microwave crosstalk. Considering both the crosstalk and its compensation signals applied on a TLS, the Hamiltonian in the laboratory frame ($\hbar = 1$) is

$$H = -\frac{\omega_{TLS}}{2}\sigma_z + \Omega\cos(\omega_{cr}t + \varphi)\sigma_x \tag{1}$$

 doi:10.20944/preprints202403.1706.v2

where $\sigma_{x,y,z}$ are Pauli matrixes, ω_{TLS} takes the value of ω_{ge} in the computational subpace, and ω_{ef} in the $\{|e\rangle, |f\rangle\}$ subspace. Ω (φ) is the effective drive amplitude (phase) under the action of Ω_{cr} and Ω_{com}. The simple trigonometric formula gives

$$\Omega = \sqrt{\Omega_{\mathrm{com}}^2 + \Omega_{\mathrm{cr}}^2 + 2\Omega_{\mathrm{com}}\Omega_{\mathrm{cr}}\cos(\phi_{\mathrm{com}} - \phi_{\mathrm{cr}})} \tag{2a}$$

$$\varphi = \arctan \frac{\Omega_{\mathrm{com}} \sin\phi_{\mathrm{com}} + \Omega_{\mathrm{cr}} \sin\phi_{\mathrm{cr}}}{\Omega_{\mathrm{com}} \cos\phi_{\mathrm{com}} + \Omega_{\mathrm{cr}} \cos\phi_{\mathrm{cr}}} \tag{2b}$$

Moving to the rotation frame and with the rotation wave approximation, we have

$$H_R = \frac{\Delta}{2}\sigma_z + \frac{\Omega}{2}\left[\cos(\varphi)\sigma_x - \sin(\varphi)\sigma_y\right] \tag{3}$$

where, $\Delta = \omega_{\mathrm{cr}} - \omega_{\mathrm{TLS}}$ is the detuning between TLS and crosstalk signal. Eq. (3) is simply an off-resonant Rabi model, which we used to model all kinds of crosstalk scenarios. The effective Rabi strength $\Omega_R = \sqrt{\Delta^2 + \Omega^2}$, and the corresponding rotation axis is $(\sin\theta\cos\varphi, \sin\theta\sin\varphi, \cos\theta)$ with $\theta = \arctan(\Omega/\Delta)$, see Figure1(b).

We classify microwave crosstalk into two different types. The first type is the far-off-resonant case, $\Delta \gg \Omega$, $\theta \approx 0$; the crosstalk mainly induces phase error that is better observed in the **XY** plane. We thus use the $X_{\pi/2}$ Ramsey-like sequence to prepare the qubit in the equatorial plane and measure it on the basis of σ_y, as shown in Figure2(a). The excited state probability P_1 of the final state is

$$P_1^{X/2} = A + (1 - A)\cos\alpha, \tag{4}$$

where $A = \left(1 + \sin^2\theta\sin^2\varphi\right)/2, \alpha = \Omega_R\tau$. Note that a simplification $\Delta\tau = 2n\pi$ is used to obtain the above equation so that the phase results from frame rotation can be ignored. For more general results, see supplementary material.

The second type is the resonant or near-resonant case, $\Delta \ll \Omega$, $\theta \approx \pi/2$; we use the X_π Ramsey-like sequence (also shown in Figure2(a)) to calibrate the crosstalk effect where amplitude or leakage error manifests. The probability P_1 in this case is

$$P_1^X = B(1 - \cos\alpha), \tag{5}$$

where $B = \sin^2\theta/2, \alpha = \Omega_R\tau$. We note that in principle, the $X_{\pi/2}$ Ramsey-like sequence can also be used for the second type, see Figure2(b), but the X_π Ramsey-like sequence provides greater contrast and sensitivity which may lead to better accuracy.

 doi:10.20944/preprints202403.1706.v2

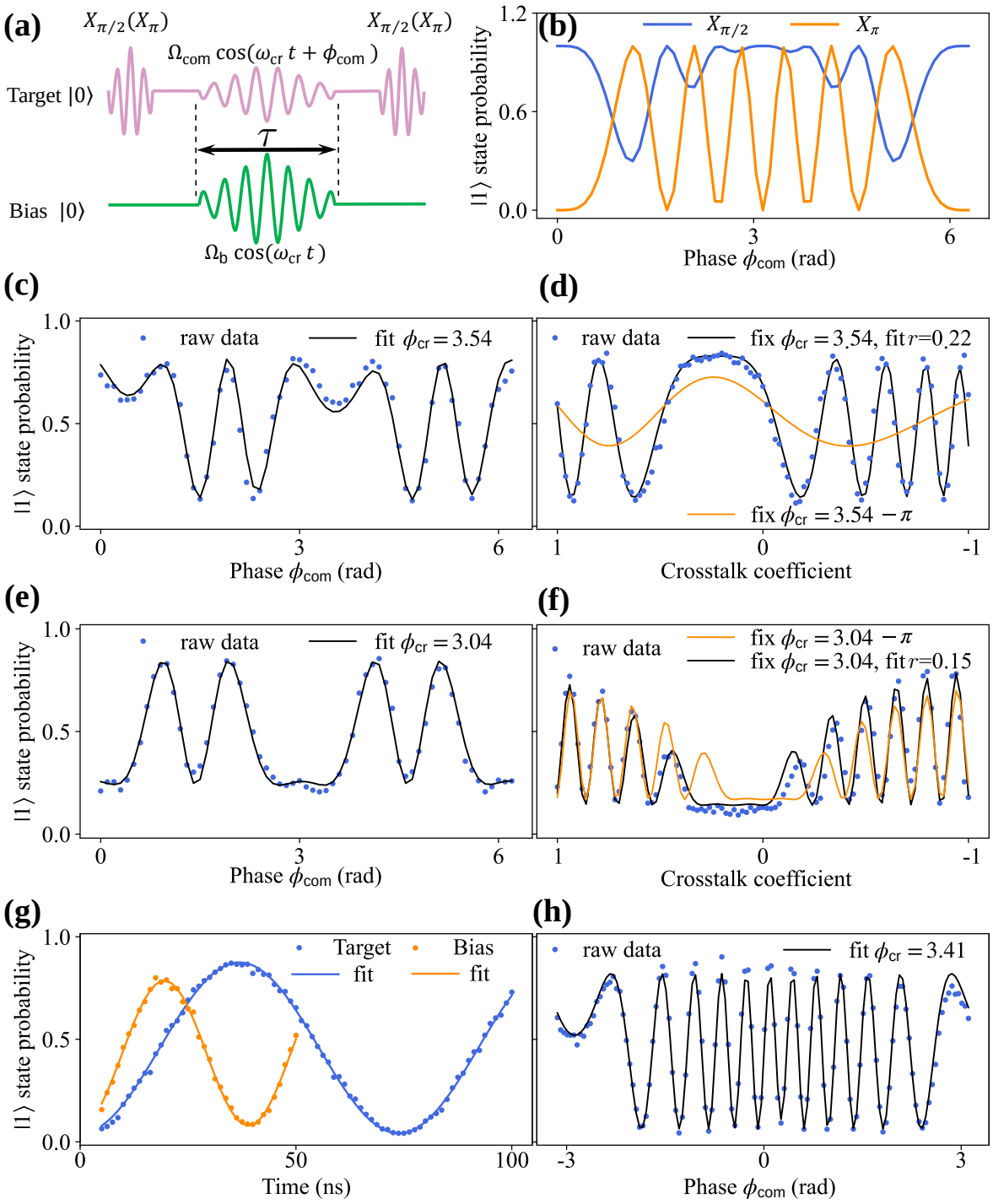

Figure 2. (a) Pulse sequence for calibrating the crosstalk in the Ramsey-like experiment. The $X_{\pi/2}$ pulse is used for the far-off-resonance case and the X_π pulse is used for the near-resonant case. (b) Simulation results for the two sequences in (a) when it is near resonance. (c), (d) Experimental results for the first type of crosstalk. (c) The fitted phase ϕ_{cr} (black line) may not necessarily be accurate. (d) Set the phase of compensation signal ϕ_{com} = 3.54-π. The experimental data obtained by scanning the coefficients (blue dots) are fitted with $\phi_{cr} = 3.54$ (black line) and $\phi_{cr} = 3.54 - \pi$ (orange line), respectively. The best-fitting result indicates $\phi_{cr} = 3.54$, and $r = 0.22$. Experimental results for scanning the crosstalk compensation phase (e) and coefficient (f) for near resonances in the leakage subspace. In (f), when fixing ϕ_{com} to $3.04 - \pi$, the experimental data obtained by scanning the coefficients (blue dots) are fitted to $\phi_{cr} = 3.04$ (black line) and $\phi_{cr} = 3.04 - \pi$ (orange line). The optimal fitting outcome indicates that ϕ_{cr} is 3.04, with a corresponding coefficient of 0.15. (g) In the case of resonance, Rabi oscillations of the target qubit $\Omega_{cr}/2\pi = 13.6$ MHz (blue) and the bias qubit $\Omega_b/2\pi = 25.6$ MHz (orange) when driven through the bias qubit local drive line are used to extract $r = \Omega_{cr}/\Omega_b = 0.531$. Then, the experimental results of scanning the phase are presented in (h) with blue points. The black line is fitted to Eq. (5) to extract ϕ_{cr}.

 doi:10.20944/preprints202403.1706.v2

In the experiment, applying a fixed amplitude drive on the bias qubit for a duration of τ, our goal is to search for the best compensation parameters on the target qubit. To avoid two-dimensional parameter scanning and improve the experimental efficiency, we fix τ and only need two sets of data of scaning Ω_{com} and ϕ_{com} successively.

For the first crosstalk type, first, the compensation signal on the target qubit is fixed to $\Omega_{\text{com}} = r\Omega_{\text{b}}$ (r is arbitrary in this step), and the experimental data of scanning its phase are fitted with Eq. (4), as shown in Figure2(c). We obtain a crosstalk phase ϕ_{cr} of 3.54; however, this phase is not necessarily accurate, especially when the difference between the two Rabi frequencies Ω_{com} and Ω_{cr} is large. At this time, the difference between $(\Omega_{\text{com}} + \Omega_{\text{cr}})^2$ and $(\Omega_{\text{com}} - \Omega_{\text{cr}})^2$ is negligible, and corresponds to a pair of opposite phases. Next, we set the compensation phase $\phi_{\text{com}} = 3.54 - \pi$, and scan r to fit with $\phi_{\text{cr}} = 3.54$ and $\phi_{\text{cr}} = 3.54 - \pi$, which are shown in Figure2(d). The phase that best fits the data is the true crosstalk signal phase, and the crosstalk coefficient is extracted to 0.22 at the same time.

For the second crosstalk type, the process aligns with that shown in Figure2(c) and (d) except for the X_π Ramsey-like sequence. Figure2(e) and (f) show an example in the leakage subspace, where ω_{cr} is close to ω_{ef}. Initially, we fix the compensation amplitude, and the experimental results (blue points) along with the fitting results (black solid line) for scanning the phase are depicted in Figure2(e), where the fitted phase with Eq. (5) is 3.04. Subsequently, similar to the previous procedure, we fix the compensation phase at $\phi_{\text{com}} = 3.04 - \pi$ and fit the experimental results with $\phi_{\text{cr}} = 3.04$ and $\phi_{\text{cr}} = 3.04 - \pi$, respectively, based on Eq.(5), as shown in Figure2(f). Ultimately, we determine that the phase of the crosstalk signal is 3.04, and the crosstalk coefficient is 0.15. Finally, we note that when the crosstalk signal is exactly in resonance with the qubit frequency, the above procedure is applicable, but there is a simple method worth noting. The crosstalk coefficient r can be directly obtained by measuring Rabi oscillations as shown in Figure2(g) and the crosstalk phase is fitted with Eq. (5) in Fig. 2(h), applying the π Ramsey-like sequence as before.

In short, we use the Ramsey-like sequence X_π or $X_{\pi/2}$ to scan the phase and the compensation amplitude separately to obtain the correct crosstalk parameters. In the case of resonance, the crosstalk coefficient is first obtained through Rabi oscillation and then the phase is fit with the sequence X_π. This method is simple, efficient, and universal, so it is beneficial for fully automated calibration of microwave crosstalk in a large-scale quantum processor.

 doi:10.20944/preprints202403.1706.v2

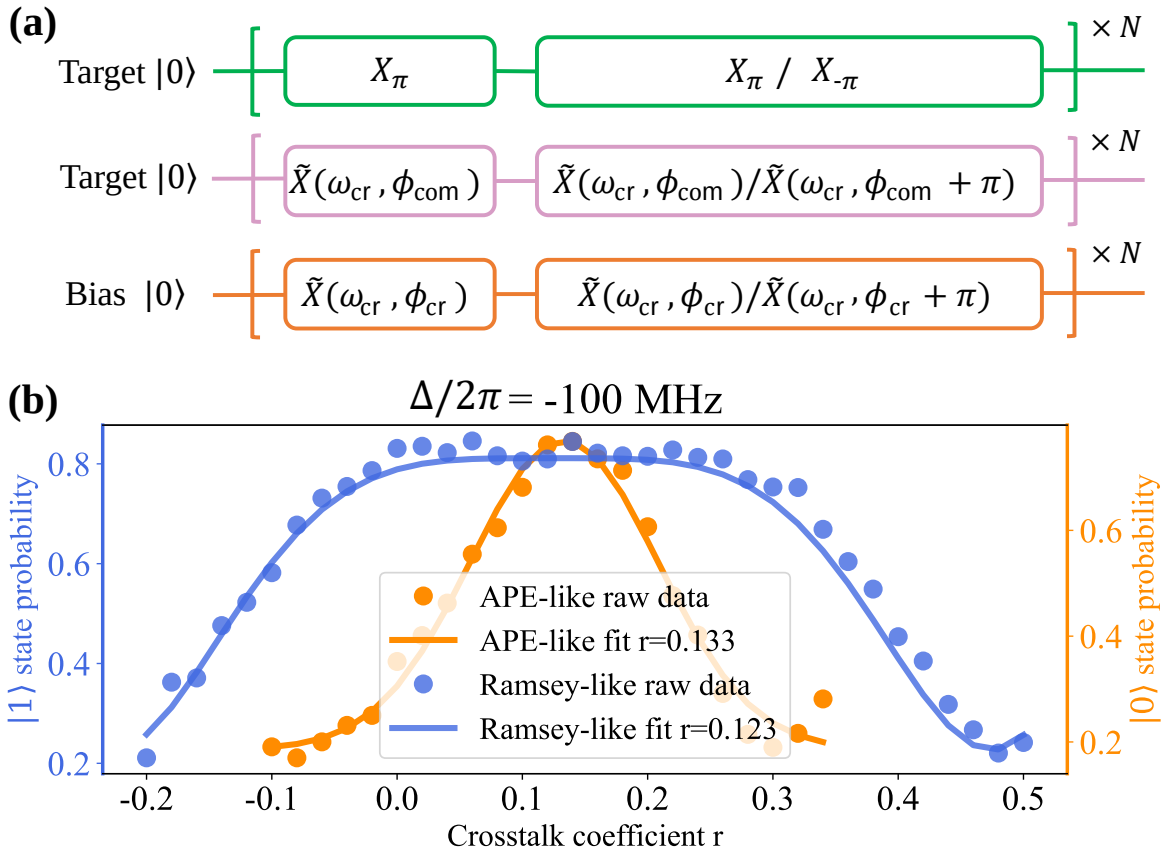

Figure 3. (a) Repeated pulse sequences of EAS. In addition to applying the driving signal of its own frequency (top) to the target qubit, a compensation signal (middle) is also added. This compensation sequence changes following the pulse sequence of the bias qubit (below). (b) Comparison of the Ramsey-like sequence (blue) and EAS (orange) results for measuring the crosstalk coefficient.

However, when the detuning is sufficiently large and not close to the anharmonicity, we observe that the experiment of sweeping the crosstalk coefficient exhibits a flat-top phenomenon near full compensation, which can also be seen in previous works. This indicates the insensitivity of the Ramsey-like experiment in the large detuning case. Therefore, we supplement the srror amplifing sequence (EAS) to fine-tune the crosstalk parameters. The pulse is depicted in Figure 3(a), where $X_\pi X_{-\pi}$ is particularly sensitive to phase error, and $X_\pi X_\pi$ can amplify amplitude error and leakage error [39]. Therefore, different pulse combinations can amplify the dominant error under different detuning conditions.

In the experiment, the frequency of the target qubit is 4799.0 MHz, and that of the bias qubit is 4699.0 MHz, with the anharmonicity of the target qubit being -232 MHz. Because the phase error is the dominant error, repeated pulse sequences $X_\pi X_{-\pi}$ are applied to the target qubit, and the corresponding crosstalk and compensation signals are applied in a similar fashion. Following this, the excited state population P_1 of the EAS experimental result and ground state population P_0 in the Ramsey-like experiment are compared in Figure3(b), indicating that the EAS is more sensitive to minor errors. In our experiments, due to the existence of distortion and other nonideal factors on the control lines, the parameters obtained from the EAS experiment perform better in multiqubit experiments.

Table 1. The frequency and anharmonicity of five qubits.

Qubit Number	q1	q2	q3	q4	q5
Frequency $\omega_{ge}/2\pi$ (MHz)	4137	4181	4524	4799	4075
Anharmonicity $\eta/2\pi$ (MHz)	-243	-223	-250	-228	-244

 doi:10.20944/preprints202403.1706.v2

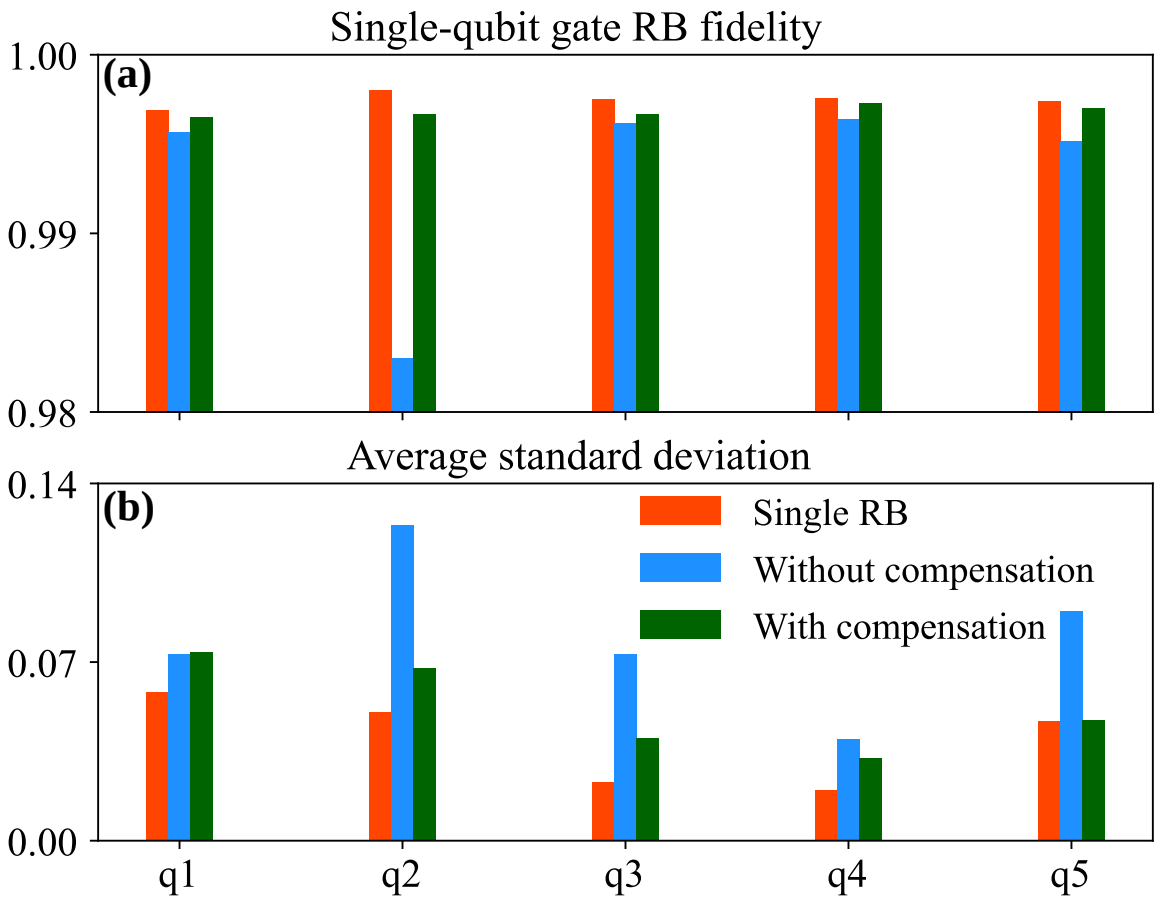

Figure 4. (a) Fidelity per single-qubit gate obtained by implementing RB separately (red), simultaneously without compensation (blue) and simultaneously with compensation (green). (b) The average standard deviation of multiple sequences repeated 30 times per sequence.

Finally, to verify the effectiveness of our method, we perform individual single-qubit-gate randomized benchmarking (RB) and simultaneous RB [40,41] with and without microwave crosstalk compensation for five qubits in a 1D chain. The frequencies and anharmonicities of the five qubits are shown in Table 1. The resulting fidelities are shown in Figure4(a), and the corresponding average standard deviation of multiple sequences repeated 30 times per sequence is shown in Figure4(b). Microwave crosstalk causes the fidelities of some qubits in the simultaneous RB to decrease, and the average standard deviation also increases significantly. Following the above experimental process, after crosstalk compensation, the fidelities and average standard deviations of the simultaneous RBs are basically close to the levels of the individual RB, confirming the effectiveness of our method for microwave crosstalk calibration.

In summary, we introduced a rapid and universally applicable calibration method for microwave crosstalk, leveraging Ramsey-like sequences that significantly enhance calibration processes in superconducting circuits. This method circumvents the complexities of traditional calibration by implementing a simplified two-level off-resonant driving model, which standardizes calibration across various crosstalk scenarios and simplifies the extraction of target parameters through one-dimensional sweeps rather than complex two-dimensional scans. Additionally, our incorporation of error-amplifying sequences notably enhances measurement accuracy, particularly in the case of significant detuning. The validity of our method has been verified through simultaneous RB, where the fidelities are recovered to the level of individual RB. Our methodology represents a significant step forward in automating the calibration process for large-scale quantum processors. This advancement is pivotal for harnessing the

 doi:10.20944/preprints202403.1706.v2

capabilities of current noisy-intermediate-scale quantum processors, paving the way for more reliable and efficient quantum computing operations.

Supplementary Materials: The following supporting information can be downloaded at the website of this paper posted on Preprints.org.

Acknowledgments: This work is supported by the National Natural Science Foundation of China (Grants No. 12034018 and No. 11625419). This work is partially carried out at the USTC Center for Micro and Nanoscale Research and Fabrication.

References

1. Preskill, J. Quantum Computing in the NISQ era and beyond. *Quantum* **2018**, *2*, 79. doi:10.22331/q-2018-08-06-79.
2. Nielsen, M.A.; Chuang, I.L. *Quantum computation and quantum information*; Cambridge university press, 2010. doi:10.1017/CBO9780511976667.
3. Shor, P.W. Polynomial-time algorithms for prime factorization and discrete logarithms on a quantum computer. *SIAM review* **1999**, *41*, 303–332. doi:10.1137/S0036144598347011.
4. Hangleiter, D.; Eisert, J. Computational advantage of quantum random sampling. *Review of Modern Physics* **2023**, *95*, 035001. doi:10.1103/RevModPhys.95.035001.
5. Zhong, H.S.; Wang, H.; Deng, Y.H.; Chen, M.C.; Peng, L.C.; Luo, Y.H.; Qin, J.; Wu, D.; Ding, X.; Hu, Y.; others. Quantum computational advantage using photons. *Science* **2020**, *370*, 1460–1463. doi:10.1126/science.abe8770.
6. Zhong, H.S.; Deng, Y.H.; Qin, J.; Wang, H.; Chen, M.C.; Peng, L.C.; Luo, Y.H.; Wu, D.; Gong, S.Q.; Su, H.; others. Phase-programmable gaussian boson sampling using stimulated squeezed light. *Physical Review Letters* **2021**, *127*, 180502. doi:10.1103/PhysRevLett.127.180502.
7. Madsen, L.S.; Laudenbach, F.; Askarani, M.F.; Rortais, F.; Vincent, T.; Bulmer, J.F.; Miatto, F.M.; Neuhaus, L.; Helt, L.G.; Collins, M.J.; others. Quantum computational advantage with a programmable photonic processor. *Nature* **2022**, *606*, 75–81. doi:10.1038/s41586-022-04725-z.
8. Arute, F.; Arya, K.; Babbush, R.; Bacon, D.; Bardin, J.C.; Barends, R.; Biswas, R.; Boixo, S.; Brandao, F.G.S.L.; Buell, D.A.; Burkett, B.; Chen, Y.; Chen, Z.; Chiaro, B.; Collins, R.; Courtney, W.; Dunsworth, A.; Farhi, E.; Foxen, B.; Fowler, A.; Gidney, C.; Giustina, M.; Graff, R.; Guerin, K.; Habegger, S.; Harrigan, M.P.; Hartmann, M.J.; Ho, A.; Hoffmann, M.; Huang, T.; Humble, T.S.; Isakov, S.V.; Jeffrey, E.; Jiang, Z.; Kafri, D.; Kechedzhi, K.; Kelly, J.; Klimov, P.V.; Knysh, S.; Korotkov, A.; Kostritsa, F.; Landhuis, D.; Lindmark, M.; Lucero, E.; Lyakh, D.; Mandrà, S.; McClean, J.R.; McEwen, M.; Megrant, A.; Mi, X.; Michielsen, K.; Mohseni, M.; Mutus, J.; Naaman, O.; Neeley, M.; Neill, C.; Niu, M.Y.; Ostby, E.; Petukhov, A.; Platt, J.C.; Quintana, C.; Rieffel, E.G.; Roushan, P.; Rubin, N.C.; Sank, D.; Satzinger, K.J.; Smelyanskiy, V.; Sung, K.J.; Trevithick, M.D.; Vainsencher, A.; Villalonga, B.; White, T.; Yao, Z.J.; Yeh, P.; Zalcman, A.; Neven, H.; Martinis, J.M. Quantum supremacy using a programmable superconducting processor. *Nature* **2019**, *574*, 505–510. doi:10.1038/s41586-019-1666-5.
9. Zhu, Q.; Cao, S.; Chen, F.; Chen, M.C.; Chen, X.; Chung, T.H.; Deng, H.; Du, Y.; Fan, D.; Gong, M.; Guo, C.; Guo, C.; Guo, S.; Han, L.; Hong, L.; Huang, H.L.; Huo, Y.H.; Li, L.; Li, N.; Li, S.; Li, Y.; Liang, F.; Lin, C.; Lin, J.; Qian, H.; Qiao, D.; Rong, H.; Su, H.; Sun, L.; Wang, L.; Wang, S.; Wu, D.; Wu, Y.; Xu, Y.; Yan, K.; Yang, W.; Yang, Y.; Ye, Y.; Yin, J.; Ying, C.; Yu, J.; Zha, C.; Zhang, C.; Zhang, H.; Zhang, K.; Zhang, Y.; Zhao, H.; Zhao, Y.; Zhou, L.; Lu, C.Y.; Peng, C.Z.; Zhu, X.; Pan, J.W. Quantum computational advantage via 60-qubit 24-cycle random circuit sampling. *Science Bulletin* **2022**, *67*, 240–245. doi:10.1016/j.scib.2021.10.017.
10. Wu, Y.; Bao, W.S.; Cao, S.; Chen, F.; Chen, M.C.; Chen, X.; Chung, T.H.; Deng, H.; Du, Y.; Fan, D.; Gong, M.; Guo, C.; Guo, C.; Guo, S.; Han, L.; Hong, L.; Huang, H.L.; Huo, Y.H.; Li, L.; Li, N.; Li, S.; Li, Y.; Liang, F.; Lin, C.; Lin, J.; Qian, H.; Qiao, D.; Rong, H.; Su, H.; Sun, L.; Wang, L.; Wang, S.; Wu, D.; Xu, Y.; Yan, K.; Yang, W.; Yang, Y.; Ye, Y.; Yin, J.; Ying, C.; Yu, J.; Zha, C.; Zhang, C.; Zhang, H.; Zhang, K.; Zhang, Y.; Zhao, H.; Zhao, Y.; Zhou, L.; Zhu, Q.; Lu, C.Y.; Peng, C.Z.; Zhu, X.; Pan, J.W. Strong Quantum Computational Advantage Using a Superconducting Quantum Processor. *Physical Review Letters* **2021**, *127*, 180501. doi:10.1103/PhysRevLett.127.180501.
11. Kim, Y.; Eddins, A.; Anand, S.; Wei, K.X.; Van Den Berg, E.; Rosenblatt, S.; Nayfeh, H.; Wu, Y.; Zaletel, M.; Temme, K.; others. Evidence for the utility of quantum computing before fault tolerance. *Nature* **2023**, *618*, 500–505. doi:10.1038/s41586-023-05657-4.

 doi:10.20944/preprints202403.1706.v2

12. Ryan-Anderson, C.; Bohnet, J.G.; Lee, K.; Gresh, D.; Hankin, A.; Gaebler, J.; Francois, D.; Chernoguzov, A.; Lucchetti, D.; Brown, N.C.; others. Realization of real-time fault-tolerant quantum error correction. *Physical Review X* **2021**, *11*, 041058. doi:10.1103/PhysRevX.11.041058.
13. Krinner, S.; Lacroix, N.; Remm, A.; Di Paolo, A.; Genois, E.; Leroux, C.; Hellings, C.; Lazar, S.; Swiadek, F.; Herrmann, J.; Norris, G.J.; Andersen, C.K.; Müller, M.; Blais, A.; Eichler, C.; Wallraff, A. Realizing repeated quantum error correction in a distance-three surface code. *Nature* **2022**, *605*, 669–674. doi:10.1038/s41586-022-04566-8.
14. Zhao, Y.; Ye, Y.; Huang, H.L.; Zhang, Y.; Wu, D.; Guan, H.; Zhu, Q.; Wei, Z.; He, T.; Cao, S.; Chen, F.; Chung, T.H.; Deng, H.; Fan, D.; Gong, M.; Guo, C.; Guo, S.; Han, L.; Li, N.; Li, S.; Li, Y.; Liang, F.; Lin, J.; Qian, H.; Rong, H.; Su, H.; Sun, L.; Wang, S.; Wu, Y.; Xu, Y.; Ying, C.; Yu, J.; Zha, C.; Zhang, K.; Huo, Y.H.; Lu, C.Y.; Peng, C.Z.; Zhu, X.; Pan, J.W. Realization of an Error-Correcting Surface Code with Superconducting Qubits. *Physical Review Letters* **2022**, *129*, 030501. doi:10.1103/PhysRevLett.129.030501.
15. Acharya, R.; Aleiner, I.; Allen, R.; Andersen, T.I.; Ansmann, M.; Arute, F.; Arya, K.; Asfaw, A.; Atalaya, J.; Babbush, R.; Bacon, D.; Bardin, J.C.; Basso, J.; Bengtsson, A.; Boixo, S.; Bortoli, G.; Bourassa, A.; Bovaird, J.; Brill, L.; Broughton, M.; Buckley, B.B.; Buell, D.A.; Burger, T.; Burkett, B.; Bushnell, N.; Chen, Y.; Chen, Z.; Chiaro, B.; Cogan, J.; Collins, R.; Conner, P.; Courtney, W.; Crook, A.L.; Curtin, B.; Debroy, D.M.; Del Toro Barba, A.; Demura, S.; Dunsworth, A.; Eppens, D.; Erickson, C.; Faoro, L.; Farhi, E.; Fatemi, R.; Flores Burgos, L.; Forati, E.; Fowler, A.G.; Foxen, B.; Giang, W.; Gidney, C.; Gilboa, D.; Giustina, M.; Grajales Dau, A.; Gross, J.A.; Habegger, S.; Hamilton, M.C.; Harrigan, M.P.; Harrington, S.D.; Higgott, O.; Hilton, J.; Hoffmann, M.; Hong, S.; Huang, T.; Huff, A.; Huggins, W.J.; Ioffe, L.B.; Isakov, S.V.; Iveland, J.; Jeffrey, E.; Jiang, Z.; Jones, C.; Juhas, P.; Kafri, D.; Kechedzhi, K.; Kelly, J.; Khattar, T.; Khezri, M.; Kieferová, M.; Kim, S.; Kitaev, A.; Klimov, P.V.; Klots, A.R.; Korotkov, A.N.; Kostritsa, F.; Kreikebaum, J.M.; Landhuis, D.; Laptev, P.; Lau, K.M.; Laws, L.; Lee, J.; Lee, K.; Lester, B.J.; Lill, A.; Liu, W.; Locharla, A.; Lucero, E.; Malone, F.D.; Marshall, J.; Martin, O.; McClean, J.R.; McCourt, T.; McEwen, M.; Megrant, A.; Meurer Costa, B.; Mi, X.; Miao, K.C.; Mohseni, M.; Montazeri, S.; Morvan, A.; Mount, E.; Mruczkiewicz, W.; Naaman, O.; Neeley, M.; Neill, C.; Nersisyan, A.; Neven, H.; Newman, M.; Ng, J.H.; Nguyen, A.; Nguyen, M.; Niu, M.Y.; O'Brien, T.E.; Opremcak, A.; Platt, J.; Petukhov, A.; Potter, R.; Pryadko, L.P.; Quintana, C.; Roushan, P.; Rubin, N.C.; Saei, N.; Sank, D.; Sankaragomathi, K.; Satzinger, K.J.; Schurkus, H.F.; Schuster, C.; Shearn, M.J.; Shorter, A.; Shvarts, V.; Skruzny, J.; Smelyanskiy, V.; Smith, W.C.; Sterling, G.; Strain, D.; Szalay, M.; Torres, A.; Vidal, G.; Villalonga, B.; Vollgraff Heidweiller, C.; White, T.; Xing, C.; Yao, Z.J.; Yeh, P.; Yoo, J.; Young, G.; Zalcman, A.; Zhang, Y.; Zhu, N. Suppressing quantum errors by scaling a surface code logical qubit. *Nature* **2023**, *614*, 676–681. doi:10.1038/s41586-022-05434-1.
16. Chen, E.H.; Yoder, T.J.; Kim, Y.; Sundaresan, N.; Srinivasan, S.; Li, M.; Córcoles, A.D.; Cross, A.W.; Takita, M. Calibrated decoders for experimental quantum error correction. *Physical Review Letters* **2022**, *128*, 110504.
17. Bluvstein, D.; Evered, S.J.; Geim, A.A.; Li, S.H.; Zhou, H.; Manovitz, T.; Ebadi, S.; Cain, M.; Kalinowski, M.; Hangleiter, D.; others. Logical quantum processor based on reconfigurable atom arrays. *Nature* **2024**, *626*, 58–65. doi:10.1038/s41586-023-06927-3.
18. Campbell, E. A series of fast-paced advances in Quantum Error Correction. *Nature Reviews Physics* **2024**, *6*, 160–161. doi:10.1038/s42254-024-00706-3.
19. Córcoles, A.D.; Kandala, A.; Javadi-Abhari, A.; McClure, D.T.; Cross, A.W.; Temme, K.; Nation, P.D.; Steffen, M.; Gambetta, J.M. Challenges and Opportunities of Near-Term Quantum Computing Systems. *Proceedings of the IEEE* **2020**, *108*, 1338–1352. doi:10.1109/JPROC.2019.2954005.
20. Winick, A.; Wallman, J.J.; Emerson, J. Simulating and Mitigating Crosstalk. *Physical Review Letters* **2021**, *126*, 230502. doi:10.1103/PhysRevLett.126.230502.
21. Klimov, P.V.; Bengtsson, A.; Quintana, C.; Bourassa, A.; Hong, S.; Dunsworth, A.; Satzinger, K.J.; Livingston, W.P.; Sivak, V.; Niu, M.Y.; others. Optimizing quantum gates towards the scale of logical qubits. *Nature Communications* **2024**, *15*, 2442. doi:10.1038/s41467-024-46623-y.
22. Sarovar, M.; Proctor, T.; Rudinger, K.; Young, K.; Nielsen, E.; Blume-Kohout, R. Detecting crosstalk errors in quantum information processors. *Quantum* **2020**, *4*, 321. doi:10.22331/q-2020-09-11-321.
23. Feng, L.; Huang, Y.Y.; Wu, Y.K.; Guo, W.X.; Ma, J.Y.; Yang, H.X.; Zhang, L.; Wang, Y.; Huang, C.X.; Zhang, C.; others. Realization of a crosstalk-avoided quantum network node using dual-type qubits of the same ion species. *Nature Communications* **2024**, *15*, 204. doi:10.1038/s41467-023-44220-z.

24. Fang, C.; Wang, Y.; Huang, S.; Brown, K.R.; Kim, J. Crosstalk suppression in individually addressed two-qubit gates in a trapped-ion quantum computer. *Physical Review Letters* **2022**, *129*, 240504. doi:10.1103/PhysRevLett.129.240504.
25. Debroy, D.M.; Li, M.; Huang, S.; Brown, K.R. Logical performance of 9 qubit compass codes in ion traps with crosstalk errors. *Quantum Science and Technology* **2020**, *5*, 034002. doi:10.1088/2058-9565/ab7e80.
26. Rudinger, K.; Hogle, C.W.; Naik, R.K.; Hashim, A.; Lobser, D.; Santiago, D.I.; Grace, M.D.; Nielsen, E.; Proctor, T.; Seritan, S.; others. Experimental characterization of crosstalk errors with simultaneous gate set tomography. *PRX Quantum* **2021**, *2*, 040338. doi:10.1103/PRXQuantum.2.040338.
27. Wei, K.; Magesan, E.; Lauer, I.; Srinivasan, S.; Bogorin, D.F.; Carnevale, S.; Keefe, G.; Kim, Y.; Klaus, D.; Landers, W.; others. Hamiltonian engineering with multicolor drives for fast entangling gates and quantum crosstalk cancellation. *Physical Review Letters* **2022**, *129*, 060501. doi:10.1103/PhysRevLett.129.060501.
28. Heinz, I.; Burkard, G. Crosstalk analysis for single-qubit and two-qubit gates in spin qubit arrays. *Physical Review B* **2021**, *104*, 045420. doi:10.1103/PhysRevB.105.085414.
29. Zhao, P.; Zhang, Y.; Li, X.; Han, J.; Xu, H.; Xue, G.; Jin, Y.; Yu, H. Spurious microwave crosstalk in floating superconducting circuits. *arXiv* **2022**, [2206.03710].
30. Wang, R.; Zhao, P.; Jin, Y.; Yu, H. Control and mitigation of microwave crosstalk effect with superconducting qubits. *Applied Physics Letters* **2022**, *121*, 152602. doi:10.1063/5.0115393.
31. Santos, A.C. Role of parasitic interactions and microwave crosstalk in dispersive control of two superconducting artificial atoms. *Phys. Rev. A* **2023**, *107*, 012602. doi:10.1103/PhysRevA.107.012602.
32. Tripathi, V.; Chen, H.; Khezri, M.; Yip, K.W.; Levenson-Falk, E.; Lidar, D.A. Suppression of crosstalk in superconducting qubits using dynamical decoupling. *Physical Review Applied* **2022**, *18*, 024068. doi:10.1103/PhysRevApplied.18.024068.
33. Koch, J.; Yu, T.M.; Gambetta, J.; Houck, A.A.; Schuster, D.I.; Majer, J.; Blais, A.; Devoret, M.H.; Girvin, S.M.; Schoelkopf, R.J. Charge-insensitive qubit design derived from the Cooper pair box. *Physical Review A* **2007**, *76*, 042319. doi:10.1103/PhysRevA.76.042319.
34. Xu, K.; Sun, Z.H.; Liu, W.; Zhang, Y.R.; Li, H.; Dong, H.; Ren, W.; Zhang, P.; Nori, F.; Zheng, D.; Fan, H.; Wang, H. Probing dynamical phase transitions with a superconducting quantum simulator. *Science Advances* **2020**, *6*, eaba4935. doi:10.1126/sciadv.aba4935.
35. Sung, Y.; Ding, L.; Braumüller, J.; Vepsäläinen, A.; Kannan, B.; Kjaergaard, M.; Greene, A.; Samach, G.O.; McNally, C.; Kim, D.; Melville, A.; Niedzielski, B.M.; Schwartz, M.E.; Yoder, J.L.; Orlando, T.P.; Gustavsson, S.; Oliver, W.D. Realization of High-Fidelity CZ and ZZ -Free iSWAP Gates with a Tunable Coupler. *Physical Review X* **2021**, *11*. doi:10.1103/PhysRevX.11.021058.
36. Yan, H.; Zhao, S.; Xiang, Z.; Wang, Z.; Yang, Z.; Xu, K.; Tian, Y.; Yu, H.; Zheng, D.; Fan, H.; Zhao, S. Calibration and cancellation of microwave crosstalk in superconducting circuits. *Chinese Physics B* **2023**, *32*, 094203. doi:10.1088/1674-1056/acdc10.
37. High-Fidelity, Frequency-Flexible Two-Qubit Fluxonium Gates with a Transmon Coupler. *Physical Review X* **2023**, *13*, 031035, [2304.06087]. doi:10.1103/PhysRevX.13.031035.
38. Nuerbolati, W.; Han, Z.; Chu, J.; Zhou, Y.; Tan, X.; Yu, Y.; Liu, S.; Yan, F. Canceling microwave crosstalk with fixed-frequency qubits. *Applied Physics Letters* **2022**, *120*, 174001. doi:10.1063/5.0088094.
39. Chen, Z. Metrology of Quantum Control and Measurement in Superconducting Qubits. PhD thesis, University of California, Santa Barbara, 2018.
40. Magesan, E.; Gambetta, J.M.; Emerson, J. Characterizing quantum gates via randomized benchmarking. *Physical Review A* **2012**, *85*, 042311. doi:10.1103/PhysRevA.85.042311.
41. Gambetta, J.M.; Córcoles, A.D.; Merkel, S.T.; Johnson, B.R.; Smolin, J.A.; Chow, J.M.; Ryan, C.A.; Rigetti, C.; Poletto, S.; Ohki, T.A.; Ketchen, M.B.; Steffen, M. Characterization of addressability by simultaneous randomized benchmarking. *Physical Review Letters* **2012**, *109*, 240504. doi:10.1103/PhysRevLett.109.240504.